

January 2005

Spectral characterization of broadband THz antennas by photoconductive mixing: toward optimal antenna design

Rajind Mendis

University of Wollongong, rajind@uow.edu.au

C. Sydlo

Technische Universitaet Darmstadt, Germany

J. Sigmund

Technische Universitaet Darmstadt, Germany

M Feiginov

Technische Universitaet Darmstadt, Germany

P. Meissner

Technische Universitaet Darmstadt, Germany

See next page for additional authors

Follow this and additional works at: <https://ro.uow.edu.au/engpapers>



Part of the [Engineering Commons](#)

<https://ro.uow.edu.au/engpapers/48>

Recommended Citation

Mendis, Rajind; Sydlo, C.; Sigmund, J.; Feiginov, M; Meissner, P.; and Hartnagel, H. L.: Spectral characterization of broadband THz antennas by photoconductive mixing: toward optimal antenna design 2005.

<https://ro.uow.edu.au/engpapers/48>

Authors

Rajind Mendis, C. Sydlo, J. Sigmund, M Feiginov, P. Meissner, and H. L. Hartnagel

Spectral Characterization of Broadband THz Antennas by Photoconductive Mixing: Toward Optimal Antenna Design

R. Mendis, C. Sydlo, *Student Member, IEEE*, J. Sigmund, M. Feiginov, P. Meissner, *Member, IEEE*, and H. L. Hartnagel, *Fellow, IEEE*

Abstract—The spectral characterization of a broadband antenna using a pump-probe photomixing continuous-wave (CW) terahertz (THz) system is presented. The high dynamic range of the system, comparable to or better than that of similar pump-probe systems reported in the literature, provides an accurate means of antenna characterization. The planar antenna exhibits a log-periodic behavior at low frequencies, a bow-tie behavior at high frequencies, and a resonance characteristic in between, well in agreement with the antenna geometry. It is predicted that an improved geometry that extends the log-periodic behavior to higher frequencies would contribute significantly in enhancing the broadband performance of antenna-coupled photomixers.

Index Terms—Bow-tie antenna, log-periodic antenna, photomixing, terahertz (THz).

I. INTRODUCTION

FOR OVER a decade now, optoelectronic systems have received considerable attention by the scientific community for the generation and detection of terahertz (THz) radiation, with numerous applications in spectroscopy, sensing, and imaging [1]–[6]. While most of these systems generally operate in the time domain, continuous-wave (CW) THz systems that operate in the frequency domain, based on photoconductive mixing (photomixing), are slowly gaining ground due to their superior frequency resolution and spectral brightness [7]–[9]. A CW system driven by laser diodes is also more economical and compact compared to a pulse system driven by a Ti:Sapphire laser. Furthermore, by providing access to single frequencies, it allows real-time measurements in the frequency domain. Coupled with a photoconductive detection scheme that provides both amplitude and phase information, the complete system operates at room temperature. These properties make it ideal for high-resolution spectroscopy, CW imaging, and other frequency-domain applications.

The performance of a broadband system is greatly influenced by the transmitter (Tx) and receiver (Rx) antennas, and this paper examines the antenna behavior via the frequency response

Manuscript received July 15, 2004; revised January 21, 2005. This work was supported by the DFG, the Alexander von Humboldt Foundation, and the ZIP program of the German government.

R. Mendis is with the Faculty of Engineering, University of Wollongong, Wollongong, NSW 2522, Australia (e-mail: rajind@uow.edu.au).

C. Sydlo, J. Sigmund, M. Feiginov, P. Meissner, and H. L. Hartnagel are with the Institut fuer Hochfrequenztechnik, Technische Universitaet Darmstadt, 64283 Darmstadt, Germany.

Digital Object Identifier 10.1109/LAWP.2005.844650

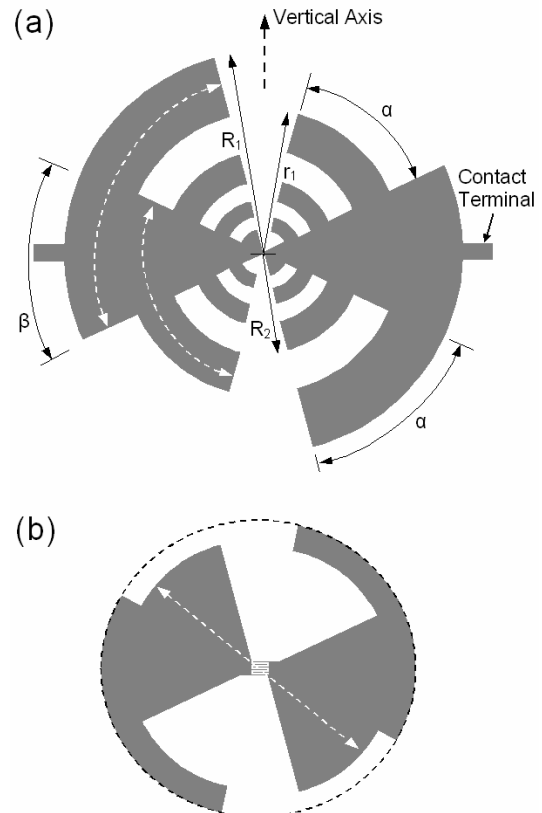


Fig. 1. Broadband THz antenna (a) with a close-up view of the central portion (b) showing the finger-photomixer at the feed-point.

of the system. To the best of our knowledge, this is the first time, antennas of this geometry, integrated with low-temperature-grown GaAs-based interdigitated finger photomixers [7] have been used for both emission and detection in the same CW THz system configuration, and investigated in this manner. In comparison to a pulse THz system where the optical pulse shape significantly affects the overall frequency response, even to the extent of masking antenna resonance behavior [10], the frequency response of a CW THz system can be made almost immune to the optical excitation, thereby providing a better means of antenna characterization.

II. ANTENNA GEOMETRY & EXPERIMENTAL SETUP

Identical antennas with the planar geometry shown in Fig. 1 are used both as the Tx and Rx in the experimental setup shown

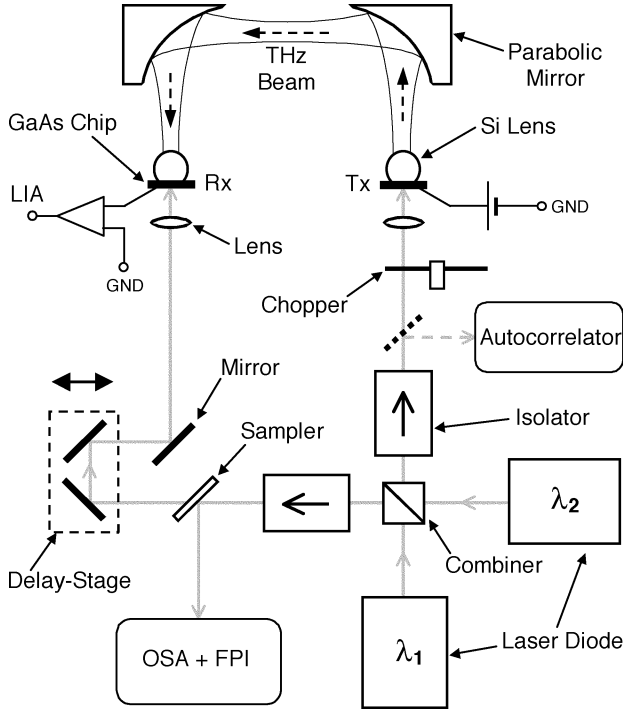


Fig. 2. Photomixing CW THz setup. Grey lines denote laser beams.

in Fig. 2. The antenna has a log-periodic circular-toothed structure, with an outer diameter of 1.28 mm; $\alpha = \beta = 50^\circ$, where α is the tooth angle, and β is the bow angle; and $\tau = \sigma^2 = 0.5$, where τ is the ratio of the radial sizes of successive teeth ($= R_{n+1}/R_n$), and σ is the size ratio of tooth and anti-tooth ($= r_n/R_n$). The innermost portion of the structure, shown in Fig. 1(b), has a bow-tie geometry with a bow angle of 100° .

As shown in Fig. 2, the system is optically driven by two laser diodes ($\lambda \approx 830$ nm), one of which is tuned to provide a THz difference-frequency. The laser beams are spatially combined, and part (pump) of the combined output illuminates the Tx photomixer, while the other part (probe) illuminates the Rx photomixer via a delay-stage. This illumination modulates the photoconductance of both Tx and Rx in synchronization at the THz beat frequency. A bias voltage applied to the Tx generates an ac photocurrent that drives the antenna. The generated CW THz radiation is coupled out by a Si lens abutted to the substrate-side of the GaAs chip, and guided toward the Rx via two parabolic mirrors. At the Rx, this radiation is coupled in to the antenna by another similar Si lens, which induces an ac voltage proportional to the received electric field. Together with the modulated photoconductance, this generates a dc current proportional to $\cos(2\pi fd/c)$, where f is the difference-frequency, d is the optical path length difference between the pump and probe beams, and c is the velocity of light. This is equivalent to homodyne detection, where the Rx local oscillator is synchronized to the frequency of the incoming (carrier) signal. Excess Rx noise is overcome by mechanically chopping the pump beam and measuring the current using a lock-in amplifier (LIA). By varying the path length difference and recording the Rx current, the complete time-dependence of the electric field is obtained. The difference-frequency is measured using an optical spectrum analyzer (OSA). A Fabry-Perot interferometer (FPI)

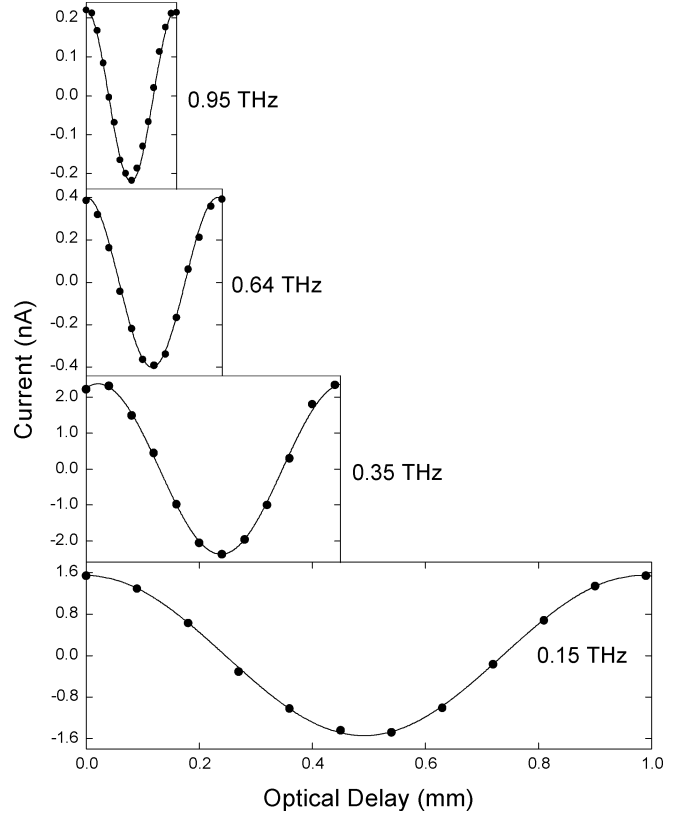


Fig. 3. Rx current versus delay-stage translation ($= d/2$). Zero optical delay is arbitrary. Vertical axes are not to scale.

and an autocorrelator monitor the spectral-mode purity and optical mixing efficiency, respectively.

III. RESULTS AND DISCUSSION

Fig. 3 shows typical scans of the Rx current for the frequencies of 0.15, 0.35, 0.64, and 0.95 THz, where the experimental values (dots) are compared against the sinusoidal expression stated above. The excellent agreement between theory and experiment signifies the high detection signal-to-noise (S:N) ratio that was better than 1000:1 at 0.35 THz with a time-constant of 300 ms and a chopper-speed of 1.25 kHz. This S:N ratio is either comparable to [9] or better than [8] what is reported in the literature for similar pump-probe CW THz systems. The data (dots) in Fig. 4 give the measured amplitude of the Rx current (proportional to the electric field amplitude) as a function of the difference-frequency, and provide the frequency response of the THz system. These data points were obtained by dithering the delay-stage and recording the peak signal at each frequency point. These points do not directly correlate to the scans in Fig. 3, and were obtained separately under strict experimental conditions in one run. As the laser is tuned, the optical power as well as the optical mixing efficiency varies, and therefore, these have to be monitored and controlled to guarantee the same optical input conditions at each frequency point. The optical powers on the Tx and Rx were held constant at 27.5 mW and 18 mW, respectively, with a mixing efficiency close to 95% on the Tx side, throughout the experiment. The dc photocurrent on the Tx was $\approx 370 \mu\text{A}$ at a bias voltage of 20 V. The data

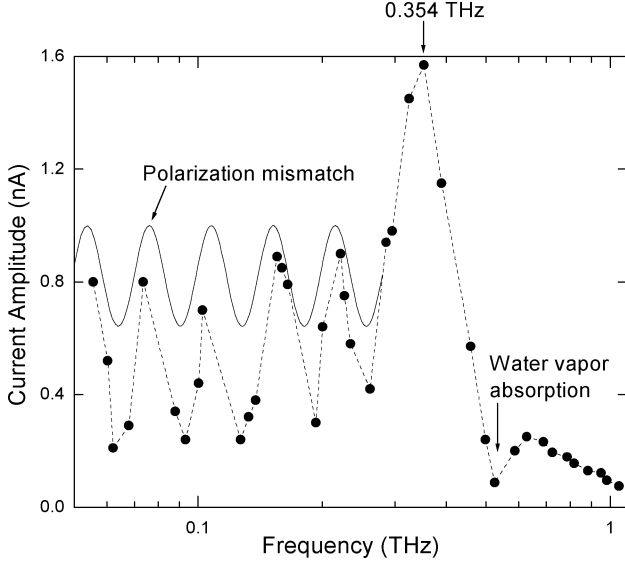


Fig. 4. Frequency response. Data points are interconnected by dashed lines. The solid periodic line gives the coupling coefficient due to the polarization mismatch.

on the semilog scale show a periodic ripple with a relatively flat peak response up to about 0.3 THz at the low-frequency end, and a smooth rolloff at the high-frequency end, with a sharp peak at about 0.35 THz. The dip near 0.5 THz is probably due to water vapor absorption [2].

The spectral features seen in Fig. 4 can be interpreted analytically based on the antenna geometry, as a combination of log-periodic and bow-tie behavior. As stated in [11], the log-periodic structure is resonant when the arc lengths [white dashed lines in Fig. 1(a)] are equal to $\lambda_g/2$, or alternatively, when the tooth arc lengths are equal to $\lambda_g/4$, as in [12]. Here, $\lambda_g = \lambda_o(\epsilon_{\text{eff}})^{-1/2}$, with $\epsilon_{\text{eff}} = (\epsilon_r + 1)/2$, where λ_o is the free-space wavelength, and ϵ_r is the relative permittivity (13 for GaAs). Following the geometric model presented in [12], the (linear) polarization associated with the log-periodic behavior undergoes a periodic tilting with the logarithm of frequency, where the extreme limits of the tilt angle correspond to the situations when the antenna is radiating from the center of a tooth, where the more dominant transverse current is localized (actually radiating from a pair of teeth on the left and right sections of the structure). As the frequency is scanned continuously, the radiation mechanism alternates between the top and bottom teeth and results in an approximately $\pm 25^\circ$ polarization-direction change, relative to the vertical direction. The polarization is vertical when the log-periodic antenna is radiating from both top and bottom teeth during the transition of the resonance. As a result of the log-periodic geometry, not only the polarization, but also the feed-point impedance, and even the radiation pattern has this periodic behavior. Since the Tx and Rx antennas in the setup have identical geometries with their planes vertical and oriented similarly as in Fig. 1, the frequency dependent tilting of the polarization causes a periodic mismatch that affects the coupling efficiency. This mismatch would be worse at frequencies corresponding to the extreme tilt angles, and zero at frequencies where the polarization is vertical. The resonance frequencies corresponding to the centers of the biggest (top) and smallest (bottom) teeth are 60

and 336 GHz, respectively. Fig. 4 also plots the amplitude-coupling coefficient (solid curve) due to the polarization mismatch, based on this simple geometric model, where the first valley is situated at 64 GHz, slightly shifted from 60 GHz, for better comparison. This curve also has a log-periodic dependence with frequency, where the *periodic ratio* is $\sqrt{2}(= 1/\sigma)$. With the $\approx 7\%$ shift in the first valley (implying a slight reduction in arc length), all the valleys and peaks of this curve agree well with the measured data, strengthening the analysis. The relative deviations are probably due to similar variations in the feed-point impedance and the radiation pattern, as well as cross-polarization effects that need to be taken into account in the theoretical curve.

The inner boundary of the smallest tooth corresponds to a frequency of 406 GHz, and may seem to be the theoretical upper limit of the log-periodic behavior, although the experimental data depicting a sharp peak at 0.35 THz dictates otherwise. This seemingly contrasting behavior can be explained by a more dominant radiation mechanism that kicks in, i.e., a $\lambda/2$ resonance condition experienced by the (radial) currents due to the termination of the bow-tie geometry at the center of the structure as seen in Fig. 1(b). This resonant length, indicated by the white dashed line, corresponds to a frequency of 354 GHz, and is in excellent agreement with measurements. As this behavior is similar to that of a resonant dipole antenna (with a much higher impedance compared to a broadband antenna such as a log-periodic or bow-tie), there is a strong signal at this frequency, irrespective of the possible mismatch in polarization and radiation patterns due to the angular orientation in space.

Beyond this frequency range, toward the high-frequency end, the structure basically behaves as a bow-tie antenna. The broadband behavior seen in the experimental results, which shows a smooth rolloff without any ripples, is consistent with this argument. The high-frequency rolloff is probably due to the finite carrier-lifetime or the RC time-constant, or a combination of both [10], where C is the parasitic capacitance of the photomixer, and R is the antenna impedance. The significant drop in signal level, compared to the log-periodic signal level (although the impedance in both cases should be close to the self-complementary value of 71Ω), can be attributed to poor coupling efficiency due to the widely spread double-lobed radiation pattern [10], [13], worsened by the mismatch in spatial orientation, and polarization.

The alignment sensitivity associated with the free-space optical beams in the THz system precludes the measurement of the antenna radiation pattern, as this requires a relative motion between the Tx and Rx that would disturb the optical beam alignment. This is in contrast to systems operating at low frequencies, where optical excitation is not required [12], [14]. One way of getting around this would be to use a fiber-coupled arrangement. However, this would be at the expense of optical pump power and considerable system modifications, and is outside the scope of this study.

IV. CONCLUSION

A pump-probe photomixing CW THz system has been used to spectrally characterize a broadband antenna. The antenna ex-

hibits a log-periodic behavior at low frequencies, and a bow-tie behavior at high frequencies, with a strong resonance behavior in between, well in agreement with the antenna geometry. As described in [7], a previous study employing an identical antenna-coupled photomixer demonstrated an output power level (measured only at 0.5 THz) within an order of magnitude of the state of the art. Based on the frequency response presented here, it is clear that this power level corresponds to a value when the antenna had changed over its behavior from a log-periodic to a bow-tie, thus limiting the usable output power. Therefore, an antenna geometry consisting of more teeth in the central portion that extends the log-periodic behavior to higher frequencies would contribute significantly in improving the broadband performance of the antenna-coupled photomixer, challenging the state of the art.

ACKNOWLEDGMENT

The authors would like to thank D. Grischkowsky and A. Cheville of Oklahoma State University for providing Si lenses.

REFERENCES

- [1] P. R. Smith, D. H. Auston, and M. C. Nuss, "Subpicosecond photoconducting dipole antennas," *IEEE J. Quantum Electron.*, vol. 24, no. 2, pp. 255–260, Feb. 1988.
- [2] M. van Exter, C. Fattinger, and D. Grischkowsky, "Terahertz time-domain spectroscopy of water vapor," *Opt. Lett.*, vol. 14, pp. 1128–1130, 1989.
- [3] Q. Wu, F. G. Sun, P. Campbell, and X.-C. Zhang, "Dynamic range of an electro-optic field sensor and its imaging applications," *Appl. Phys. Lett.*, vol. 68, pp. 3224–3226, 1996.
- [4] P. U. Jepsen, R. H. Jacobsen, and S. R. Keiding, "Generation and detection of terahertz pulses from biased semiconductor antennas," *J. Opt. Soc. Amer. B*, vol. 13, pp. 2424–2436, 1996.
- [5] L. Duvillaret, F. Garet, and J. L. Coutaz, "A reliable method for extraction of material parameters in terahertz time-domain spectroscopy," *IEEE J. Sel. Topics Quantum Electron.*, vol. 2, no. 3, pp. 739–746, Sep. 1996.
- [6] D. Mittleman, *Sensing with Terahertz Radiation*. Heidelberg, Germany: Springer-Verlag, 2002.
- [7] R. Mendis, C. Sydlo, J. Sigmund, M. Feiginov, P. Meissner, and H. L. Hartnagel, "Tunable CW-THz system with a log-periodic photoconductive emitter," *Solid State Electron.*, vol. 48, pp. 2041–2045, 2004.
- [8] K. J. Siebert, H. Quast, R. Leonhardt, T. Löffler, M. Thomson, T. Bauer, H. G. Roskos, and S. Czasch, "Continuous-wave all-optoelectronic terahertz imaging," *Appl. Phys. Lett.*, vol. 80, pp. 3003–3005, 2002.
- [9] S. Verghese, K. A. McIntosh, S. Calawa, W. F. Dinatale, E. K. Duerr, and K. A. Molvar, "Generation and detection of coherent terahertz waves using two photomixers," *Appl. Phys. Lett.*, vol. 73, pp. 3824–3826, 1998.
- [10] M. Matsuura, M. Tani, and K. Sakai, "Generation of coherent terahertz radiation by photomixing in dipole photoconductive antennas," *Appl. Phys. Lett.*, vol. 70, pp. 559–561, 1997.
- [11] M. M. Gitin, F. W. Wise, G. Arjavalingam, Y. Pastol, and R. C. Compton, "Broad-band characterization of millimeter-wave log-periodic antennas by photoconductive sampling," *IEEE Trans. Antennas Propag.*, vol. 42, no. 3, pp. 335–339, Mar. 1994.
- [12] B. K. Kormanyos, P. H. Ostdiek, W. L. Bishop, T. W. Crowe, and G. M. Rebeiz, "A planar wideband 80–200 GHz subharmonic receiver," *IEEE Trans. Microwave Theory Tech.*, vol. 41, no. 10, pp. 1730–1737, Oct. 1993.
- [13] R. C. Compton, R. C. McPhedran, Z. Popovic, G. M. Rebeiz, P. P. Tong, and D. B. Rutledge, "Bow-tie antennas on a dielectric half-space: theory and experiment," *IEEE Trans. Antennas Propag.*, vol. 35, no. 6, pp. 622–631, Jun. 1987.
- [14] C. Sydlo, B. Koegel, O. Cojocari, H. L. Hartnagel, and P. Meissner, "Characterization of a circularly-toothed planar logarithmic-periodic antenna for broadband power detection," *Frequenz*, vol. 58, pp. 207–210, 2004.